

RT-SRTS: Angle-Agnostic Real-Time Simultaneous 3D Reconstruction and Tumor Segmentation from Single X-Ray Projection

Miao Zhu, B.S.^{1, #}, Qiming Fu, M.S.^{1, #}, Bo Liu, Ph.D.^{1, *}, Mengxi Zhang¹, Bojian Li¹, Xiaoyan Luo, Ph.D.^{1, *}, Fugen Zhou, Ph.D.¹,

¹ Image Processing Center, Beihang University, Beijing 100191, People's Republic of China

Miao Zhu and Qiming Fu contributed equally

*Corresponding Author:

Bo Liu, Ph.D.

Image Processing Center

Beihang University, Beijing, 100191, P.R. China

Email: bo.liu@buaa.edu.cn

Xiaoyan Luo, Ph.D.

Image Processing Center

Beihang University, Beijing, 100191, P.R. China

Email: luoxy@buaa.edu.cn

Last revised: October 12, 2023

Abstract

Radiotherapy is one of the primary treatment methods for tumors, but the organ movement caused by respiratory motion limits its accuracy. Recently, 3D imaging from single X-ray projection receives extensive attentions as a promising way to address this issue. However, current methods can only reconstruct 3D image without direct location of the tumor and are only validated for fixed-angle imaging, which fails to fully meet the requirement of motion control in radiotherapy. In this study, we propose a novel imaging method RT-SRTS which integrates 3D imaging and tumor segmentation into one network based on the multi-task learning (MTL) and achieves real-time simultaneous 3D reconstruction and tumor segmentation from single X-ray projection at any angle. Futhermore, we propose the attention enhanced calibrator (AEC) and uncertain-region elaboration (URE) modules to aid feature extraction and improve segmentation accuracy. We evaluated the proposed method on ten patient cases and compared it with two state-of-the-art methods. Our approach not only delivered superior 3D reconstruction but also demonstrated commendable tumor segmentation results. The simultaneous reconstruction and segmentation could be completed in approximately 70 ms, significantly faster than the required time threshold for real-time tumor tracking. The efficacy of both AEC and URE was also validated through ablation studies. Our code will be available at <https://github.com/ZywooSimple/RT-SRTS>.

Keywords: 3D reconstruction, Tumor segmentation, X-ray projection, Radiotherapy,

Deep learning

1 Introduction

Lung cancer is currently the leading cause of cancer-related deaths worldwide.

Radiotherapy is considered as one of the primary treatment modalities for cancer patients, with approximately 77% of lung cancer patients requiring it with evidence-based indication[1]. However, in the case of lung cancer radiotherapy, the natural motion of tumors caused by respiration can significantly affect the efficacy of the treatment[2]. Therefore, real-time monitoring of the tumor during treatment is vital to enable respiratory-gated or tumor-tracking radiotherapy[3]. Additionally, obtaining time-resolved 3D images is necessary to accurately assess the received radiation dose for the patient[4, 5], which can greatly improve treatment outcomes.

Tumor monitoring has been extensively researched for decades[6, 7]. Currently, the most commonly used and proven techniques are marker and surrogate-based methods. However, they suffer from accuracy decline caused by marker migration or varying relations between surrogates and the target[5, 8]. Additionally, implanting markers complicates the radiotherapy protocol and may result in clinical complications such as pneumothorax[8]. As a result, there has been extensive attention on markerless monitoring of tumors based on intraoperative images. Of all available imaging modalities, kV X-ray projection is more desirable as it is easily accessible via the imaging system integrated with the linear accelerator (LINAC) radiotherapy machine,

and has better image quality than other integrated imaging modalities[9]. However, due to its perspective characteristics, it is very difficult to directly locate the tumor position from X-ray projection and is considered as "Holy Grail" in the field of image guidance for radiotherapy[9]. Moreover, the task is further complicated by the requirement of the advanced volumetric-modulated arc therapy (VMAT) modality which is widely used for lung cancer radiotherapy. Since the treatment head and imaging system rotates around the patient during treatment, it is only possible to acquire one X-ray projection at a certain angle. In this case, for motion management of VMAT, the goal becomes very complicated as it involves simultaneously reconstructing the 3D CT image and locating the tumor position based on one X-ray projection at an arbitrary angle in real-time.

One kind of method for locating tumors focuses on directly analyzing and processing X-ray projections[10-12], whose accuracy depend on the visibility and clarity of the tumor in the image. When the tumor is relatively small or blocked by other high-density substances, positioning accuracy is difficult to ensure[4]. Deep learning techniques may help tackle this issue, but efficacy is only validated on digital phantoms[8]. Moreover, obtaining time-resolved 3D images or 3D tumor position via this method is not straightforward. Other methods involve matching or registering pretreatment 3D/4D CT with the X-ray projection, which theoretically could obtain both the tumor position and time-resolved 3D CT images[9, 13-15]. However, registration of 3D images with one X-ray projection is a very ill-conditioned problem.

Simplifying the motion model or using prior motion knowledge is necessary to ensure the robustness and feasibility of the derived motion. Principal component analysis-based motion model (PCA-MM)[16] is one such method that has been successfully applied. With PCA-MM, the registration problem is reduced to optimization of several parameters, greatly reducing complexity and improving robustness[17]. However, iterative optimization is still needed, which cannot meet real-time requirements[18]. Additionally, these methods can only obtain a linear combination of a few motion principal components, making it difficult to deal with variation in respiratory motion patterns or patient position[19, 20].

Because of its powerful nonlinear modeling ability, convolutional neural network (CNN) has been recently studied for real-time 3D imaging based on X-ray projection. As one of the pioneer works, Wei et al[5, 21-23] propose to apply CNN to predict PCA-MM parameters and achieve real-time 3D imaging. However, the accuracy of the method is also limited by the generality of the PCA-MM. Instead of predicting PCA-MM parameters, some works try to directly predict the 3D CT from X-ray projection, which is more robust to motion variation. Shen et al[20] discovers that the reconstruction results based on a single X-ray projection are close to those using 10 X-ray projections, which verified the feasibility of 3D imaging based on a single X-ray projection. Subsequently, some works are studied with new mechanisms, such as adding confrontation loss and perceived loss[4], integrating the super-resolution reconstruction mechanism[24]. These methods utilize planning 4D CT of the same

patient to train the patient-specific CNN model for intraoperative imaging, which is suitable for radiotherapy. Besides, there are other works trying to train population-based CNN imaging model from CT of a group of patients and predict CT image for any patient from X-ray projection[25-29]. In comparison, the anatomical constraints of group data for specific patients are weak, and the 3D structural information provided by X-ray projection is limited. The reconstruction results still contain relatively larger errors in anatomical details than patient-specific methods.

Though patient-specific CNN imaging methods have shown very promising potential, they failed to meet the requirement of motion control for VMAT radiotherapy. First, current methods can only reconstruct 3D image but cannot directly realize the real-time localization of tumors. Second, these methods are only validated for fixed-angle imaging, i.e. training a CNN model for an angle, and thus cannot be utilized in VMAT in which the treatment beam and X-ray imaging system rotates during beam delivery. In view of this, in this work, a novel patient-specific CNN imaging method is proposed for angle-agnostic real-time simultaneous 3D reconstruction and tumor segmentation (RT-SRTS). These methods adopt the multi-task learning (MLT) strategy to integrate the 3D imaging and tumor segmentation into one network and can achieve simultaneous 3D reconstruction and tumor segmentation in real-time. A new attention enhanced calibrator (AEC) module is proposed to better fuse the extracted hierarchical features with the imaging and segmentation branches to obtain better 3D reconstruction and imaging results. The segmentation accuracy is further

boosted via a new uncertain-region elaboration (URE) module. The efficacy of the proposed method in the mode of angle-agnostic imaging, i.e. training a CNN model for all angles, is investigated and the results are compared with two state-of-the-art methods in both fixed-angle and angle-agnostic imaging modes. Better results are obtained by our method which demonstrates the advantage of the proposed method.

In summary, the contribution of this paper are as follows:

- 1) Real-time simultaneous 3D reconstruction and tumor segmentation are achieved via a two-branch CNN model.
- 2) This is the first work investigating direct 3D CT reconstruction from single X-ray projection at arbitrary angle based on one CNN imaging model.
- 3) Novel attention enhanced calibrator (AEC) module and uncertain-region elaboration (URE) module are proposed to improve the accuracy of the 3D imaging and tumor location.
- 4) Better results are obtained than two other state-of-the-art methods.

2 Material and methods

2.1 Angle-agnostic RT-SRTS Network

The aim of the proposed method is to simultaneously reconstruct a 3D CT image and segment the tumor in real-time, based on one X-ray projection acquired at any angle.

To achieve this, we propose to formulate the job as a multi-task learning problem which has been used successfully across many applications of machine learning.

Besides achieving multiple goals simultaneously, different tasks serve as a regulations for each other, helping to learn more general representations and reduce the chance of overfitting. Following the common MTL strategy of sharing hidden representation, RT-SRTS is designed as shown in Fig 1, in which a shared representation network is utilized to extract hierarchical semantic features from the input 2D X-ray projections and transform the learned 2D features into 3D format to achieve the transformation task from 2D to 3D. Based on this, a reconstruction sub-network and a segmentation sub-network are integrated to simultaneously reconstruct the 3D CT image and generate the tumor mask in one network.

We apply a residual-learning scheme in the representation network[30], in which the 2D residual block is used to facilitates the training process and avoids gradient vanish in back-propagation. Five 2D convolution residual blocks with different number of convolutional filters are concatenated to learn hierarchical semantic representations from 2D projections. Instance normalization is adopted as the training batch size is set to 1 because of the memory limit.

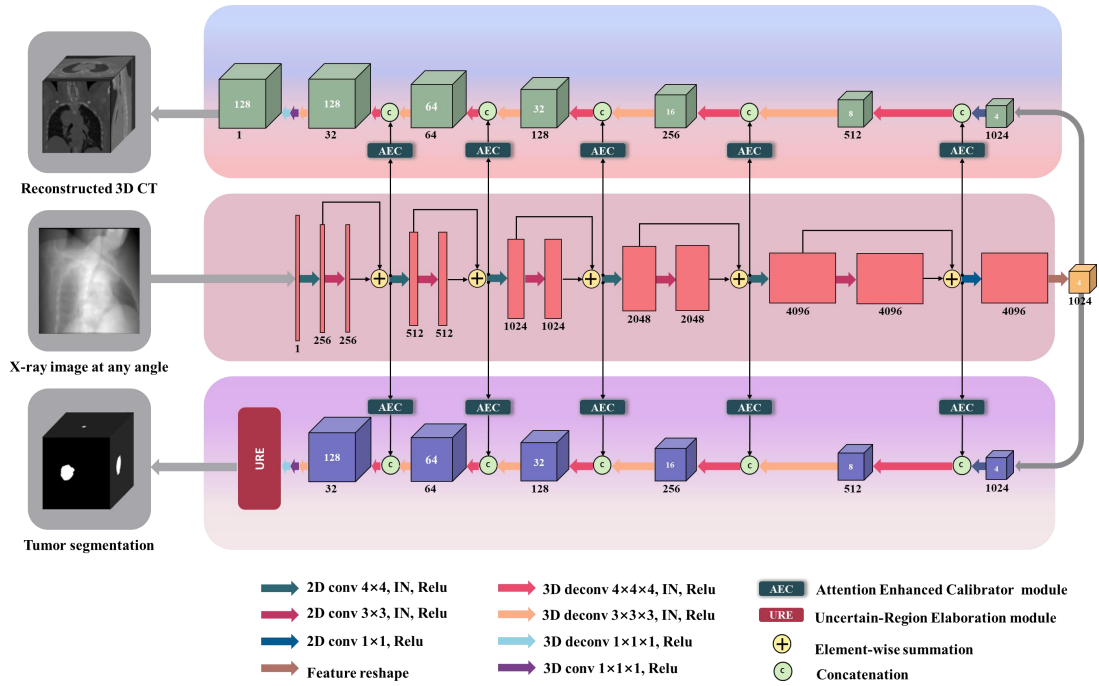


Fig 1 The framework of the proposed RT-SRTS

The CT reconstruction sub-network are built upon the 3D deconvolution block. The first deconvolution layer up-samples the feature map by a factor of 2 and accordingly reduce the number of feature maps by decreasing the number of deconvolutional filters. The second deconvolution layer performs transformation and keeps the spatial shape of 3D features. In accordance with the representation network, there are five concatenated deconvolutional blocks and a novel attention enhanced calibrator (AEC) module with attention strategy is proposed to optimally utilize the hierarchical information from the representation network.

The tumor segmentation sub-network shares a similar architecture to the CT reconstruction sub-network except for the last few layers, where a SoftMax activation function is applied on a 2-channel feature to generate the initial segmentation results. Afterwards, for the purpose of adjusting fine-grained segmentation, we finally apply

URE module at the end of the segmentation branch.

2.1.1 The attention enhanced calibrator (AEC) module

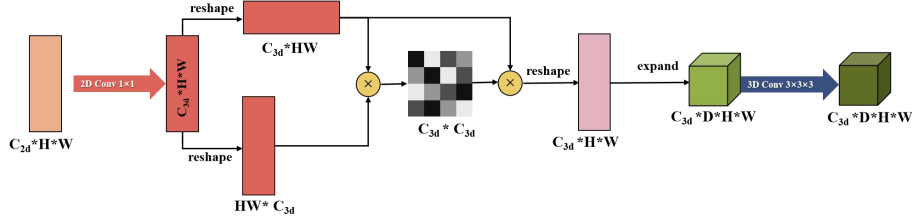


Fig 2 The architecture of the AEC module

We design the AEC module as a special skip connection to transform hierarchical features from representation sub-network to reconstruction and segmentation branches. Besides allowing for an efficient flow of gradients for learning, AEC undertakes two extra calibration functions. One is to calibrate the feature dimension, the other is to calibrate the spatial dimensions. After calibration, the output feature will have consistent dimensions both in feature and spatial domains with the concatenated 3D feature in two 3D branches.

As shown in Fig 2, for feature dimension calibration, a basic 2D convolution block is firstly applied on the input feature to compress the number of features from C_{2d} to C_{3d} . Then, we apply self-attention mechanism[31] to capture the relative relationships of various organs and tissues hidden within the features, aiming to obtain more representative features. Specifically, the correlation between features at different channels is calculated to obtain the inter-channel relationship of features, and the enhanced features with calibrated feature number ($C_{3d} * H * W$) are generated by taking

the correlation weighted sum of the all features. Finally, for spatial dimension calibration, to keep computing efficiency, a simple but effective dimension expanding is applied to copy and stack 2D feature map ($C_{3d} * H * W$) to obtain 3D feature map ($C_{3d} * D * H * W$).

2.1.2 The uncertain-region elaboration (URE) module

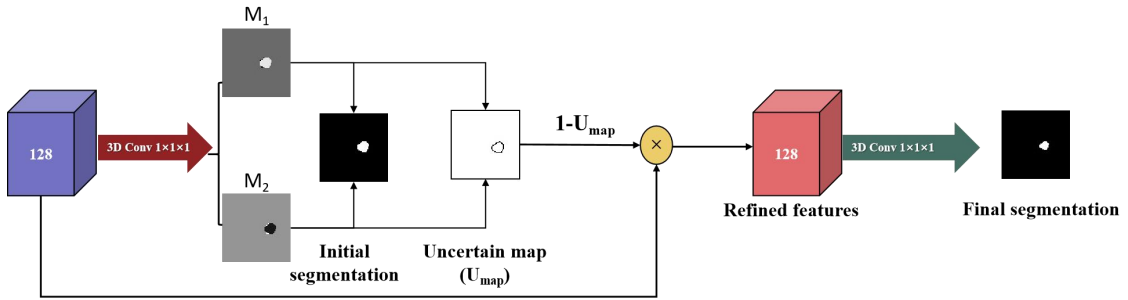


Fig 3 The uncertain-region elaboration (URE) module

The initial tumor segmentation results usually exist some blurry and uncertain regions, especially around the tumor boundaries. Inspired by recent works on uncertainty fixation[32], we propose a novel scheme, named uncertain-region elaboration (URE), to reduce the ambiguity and improve the segmentation results. It includes segmentation evaluation about such uncertainty and segmentation adjustment to obtain fine-grained results. The core idea of the URE is to leverage pixels with high confidence to rectify pixels with low confidence. Fig.3 presents the detailed structure of the URE module. After decoding and a SoftMax normalization, two probability maps M_1 and M_2 are generated to indicate the likelihood of each pixel p belonging to the tumor and background respectively. The value of M_1 and M_2 lies in $[0,1]$, and $\sum_{i=1}^2 M_i(p) = 1$. The label of p is picked by comparing M_1 and M_2 . A pixel-wise

uncertainty map U_{map} is firstly generated to measure classification ambiguity on each pixel, using the ratio of the largest likelihood value:

$$U_{map} = 1 - \exp\left(1 - \frac{\max(M_i(p))}{1 - \max(M_i(p))}\right)$$

The U_{map} has a value range of $[0,1)$, with larger U_{map} value representing more confidence. Once the uncertainty map is calculated, the initial features used for segmentation are multiplied by the U_{map} and a local convolutional operator is added to generate the refined features to obtain the final segmentation.

2.1.3 Loss function and Implementation details

Our loss function comprises two parts: MSE loss between generated and ground truth CTs and binary cross entropy (BCE) loss between the generated and the ground truth tumor masks. The weights for both losses are set to 1.0 for all cases, which are proved to be the more suitable hyperparameters.

$$L_{MSE} = \frac{1}{M \cdot N \cdot K} \sum_{i=0}^{M-1} \sum_{j=0}^{N-1} \sum_{m=0}^{K-1} (I(i, j, m) - T(i, j, m))^2$$

$$L_{BCE} = -[Y \log X + (1 - Y) \log(1 - X)]$$

$$L_{loss} = \alpha_1 L_{MSE} + \alpha_2 L_{BCE} (\alpha_1 = \alpha_2 = 1)$$

where M , N and K represents the size of 3D CT image, I and T are the generated and ground truth CT images, and X and Y denote the predicted and ground truth tumor masks.

The method is implemented based on PyTorch library and trains on a NVIDIA GeForce RTX 3090 GPU with 24 GB memory. For comparison, we use the same training strategy and hyper-parameters for all experiments. We train the network for 100 epochs; the learning rate is initially set to $2e^{-3}$ and linearly decay the learning rate after 50 epochs until reaching zero. Adam optimizer with $\beta_1=0.50$ and $\beta_2=0.99$ is used to minimize the total loss function and iteratively update network parameters through back propagation. At the end of each training epoch, the model is evaluated on the validation set and the best checkpoint model with smallest validation loss is saved.

2.2 Experimental setting

2.2.1 Training and testing data

Ten patient cases from the SPARE Challenge [33] are used to validate the proposed method. Each patient case contains a planning 4DCT with ten phases of 3DCT and the segmentation labels of the tumors sited in the thoracic or upper-abdominal regions, with each 3DCT representing the anatomic structure at a specific respiratory phase.

The training of the CNN model requires X-ray projections and their corresponding 3D CT and tumor mask, which is not available in reality. As previous works, we utilize the 3DCT at different phases derived from 4DCT to generate digitally reconstructed radiographs (DRRs) as digital simulations of X-ray projections. Specifically, at first,

all CT images and tumor labels are resampled to an isotropic resolution of $1 \times 1 \times 1$ mm³ per voxel using the cubic interpolation for CT and nearest neighbor interpolation for labels. Then, a PCA-MM is built with three principal components which are sufficient to describe most of the motion according to previous works. Based on this, 1080 DVFs are calculated by randomly sampling the PCA-MM coefficients. The corresponding CTs and tumor masks are obtained by deforming the reference CT and tumor masks with the sampled DVFs. A DRR is calculated for each CT at a random angle. A total of 1080 training samples are generated for each patient, out of which 980 samples are used for model training and the remaining 100 samples for model testing.

As previous works [25], the input and the output dimensions are set to 128×128 and $128 \times 128 \times 128$. The CT and its corresponding DRRs are resized accordingly.

Additionally, following the standard protocol of data pre-processing, we conduct scaling normalization for both the CT and DRR, with their intensity normalized to the interval [0,1].

2.4.2 Compared methods and evaluation metrics

To benchmark the proposed method, we conduct a comparative study with two methods: PatRecon[20] and X2CT[25]. These methods are compared because their codes are publicly available, which eliminates the uncertainty caused by code

implementation. Though X2CT is initially proposed as population-based imaging model taking two orthogonal X-ray projection as input, it can be easily adapted to achieve patient-specific imaging based on one X-ray projection.

As mentioned above, current methods are all designed for fixed-angle CT reconstruction. So, we conducted two types of experiments for the compared algorithms. One is the angle-agnostic imaging experiments as discussed above and the other is the fixed-angle imaging experiments. For the angle-agnostic imaging experiments, the trained models are denoted as X2CT-R and PatRecon-R. As for the fixed-angle imaging experiments, 1080 samples are generated at a fixed angle, out of which 980 random samples are used for model training and the remaining 100 samples for model testing. The trained models are denoted as X2CT-F and PatRecon-F. To illustrate the robustness of our method to angle, we only train RT-SRTS on the angle-agnostic data set and directly test the trained model on the fixed-angle data set.

The results of CT reconstruction are evaluated in terms of the mean absolute error (MAE), mean square error (MSE), root mean square error (RMSE), structural similarity measure (SSIM) and peak signal-to-noise ratio (PSNR). In practice, MAE, MSE and RMSE are commonly used to evaluate the intensity accuracy between generated and ground truth CT images, while SSIM and PSNR mainly measure the visual quality of generated CTs. As for the accuracy of tumor segmentation, the dice coefficient (DICE) and center of mass distance (COMD) is evaluated. The DICE

represents the amount of spatial overlap between the segmented and the ground truth tumor volume and the COMD measures the distance between the center of masses. In general, lower value of MAE, MSE and RMSE, and higher SSIM and PSNR indicate a better reconstruction. A higher DICE and lower COMD stand for a more precise tumor segmentation.

3 Results and discussion

3.1 Evaluation of reconstruction and segmentation performance

It takes about 15 h to train a network for 100 epochs, and the model at about 90th epoch achieves the best validation performance and uses for the test. Notably, the MSE and BCE losses are effective without requiring any weight tuning, resulting in good performance across all cases. In terms of inference speed, the trained network demonstrates efficient processing capabilities. It takes approximately 70 ms for the network to generate both the 3D image and 3D tumor mask from a single 2D projection. This processing time is significantly shorter than the maximum allowed delay time of 500 ms[3, 34], ensuring real-time tracking feasibility.

The quantitative results of CT reconstruction are presented in Fig 4. As demonstrated, RT-SRTS outperforms all other methods in terms of all metrics for the angle-agnostic experiments. For the fixed-angle imaging experiments, RT-SRTS also outperforms others in most metrics except for SSIM, albeit with a negligible difference in performance.

The CT reconstruction results are qualitatively evaluated in Fig 5. As we can see, all three methods could effectively capture tissue displacement caused by respiratory motion with similar tissue position and shape to the ground truth. However, X2CT fails to reconstruct acceptable images for angle-agnostic experiments, and generates very blurry volumes with many artefacts for fixed-angle experiments. While PatRecon achieves satisfactory reconstruction results in fixed-angle experiments, its performance significantly deteriorates in angle-agnostic experiments. This is clearly demonstrated by the highlighted area in Fig 5(a), where PatRecon-R lacks discernible fine details and struggles to differentiate tissues at close distances. Furthermore, as evident from Fig 5(b), the reconstruction results of PatRecon-R become blurred at some areas. In contrast, RT-SRTS and PatRecon-F could reconstruct the small anatomical structures better. But, in overall, the results of RT-SRTS are more clear with less noise, and approach the ground truth more closely.

exhibits similar reconstruction results to PatRecon-F in angle-agnostic experiments and approaches the ground truth more closely. Overall, the reconstruction results of RT-SRTS are clearer compared to those of PatRecon-F.

Furthermore, RT-SRTS can accurately segment the tumors with an average DICE of 0.96 ± 0.03 and an averaged COMD of 0.31 ± 0.18 mm. The 3D coordinates of the tumor are desired for tumor tracking[3] and the COMD is directly relevant with tumor

localization accuracy. The achieved results in COMD are relatively low compared with previously reported results [4] and demonstrated promising clinical value of the proposed method. Fig 6 illustrates the accuracy of RT-SRTS in terms of tumor segmentation. On each slice, there is only a small deviation in our segmentation from the ground truth.

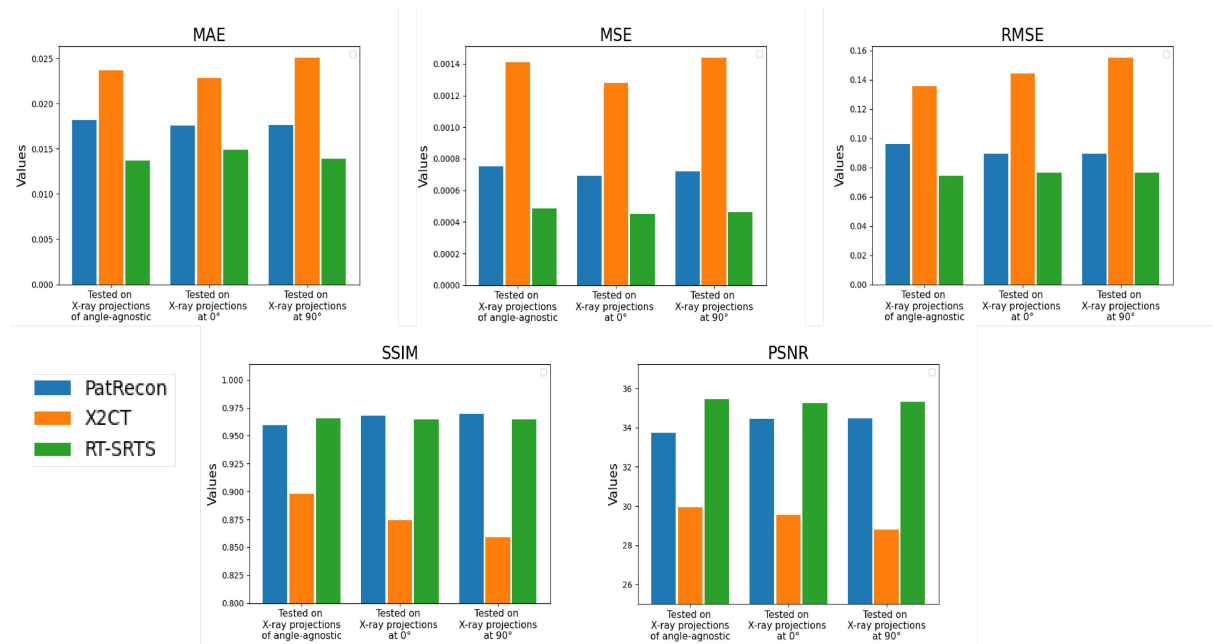
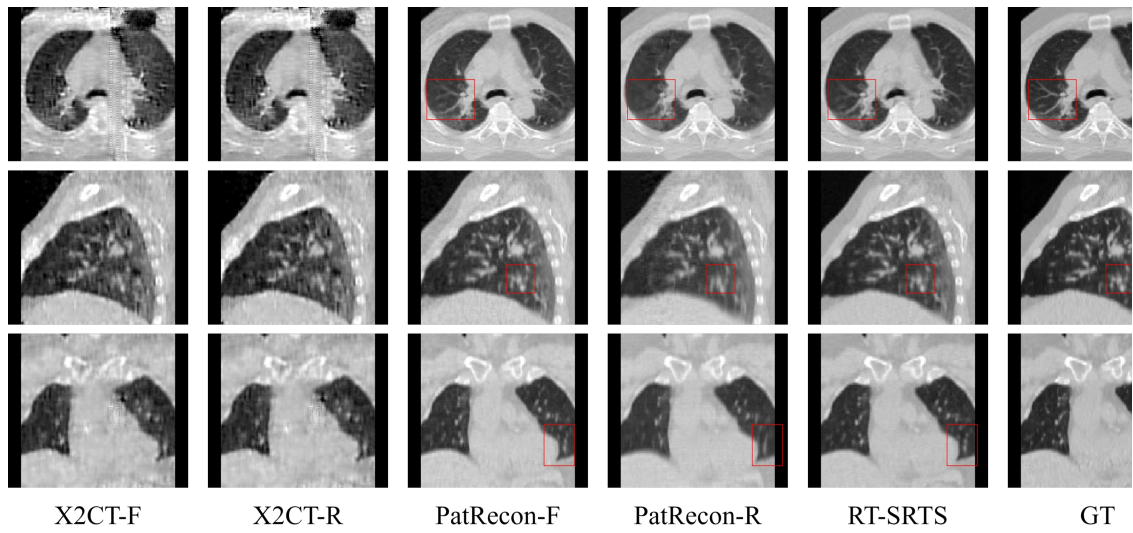
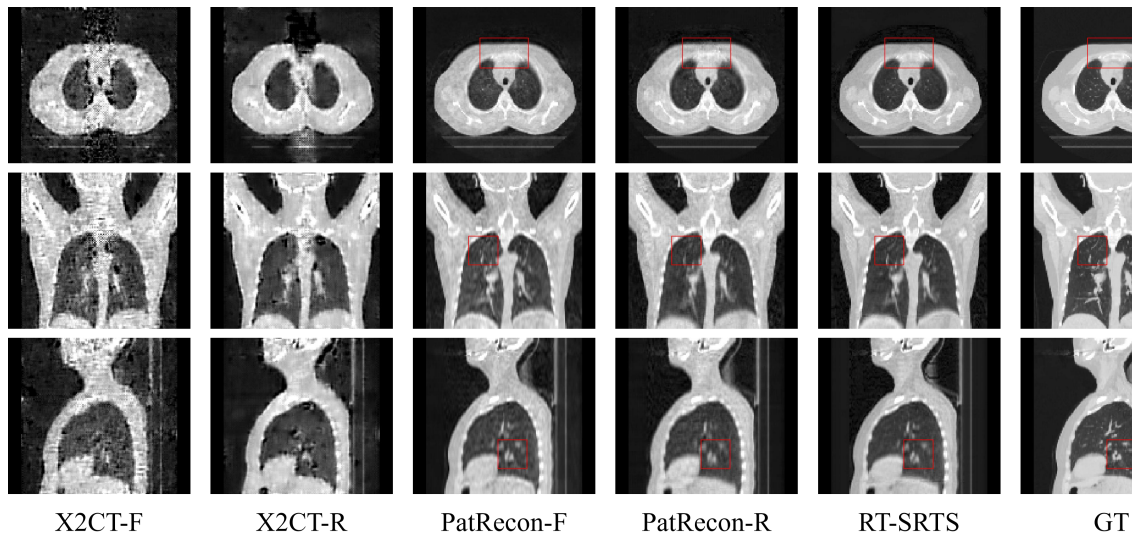


Fig 4 Quantitative comparison of different methods. It should be noted that, in fixed-angle experiments, RT-SRTS was trained in angle-agnostic setting and directly tested on the corresponding test dataset.



(a) Reconstructed lung CT image result (fixed angle at 90°)



(b) Reconstructed chest CT image result (fixed angle at 0°)

Fig 5 Visual comparison between the reconstruction results of different methods.

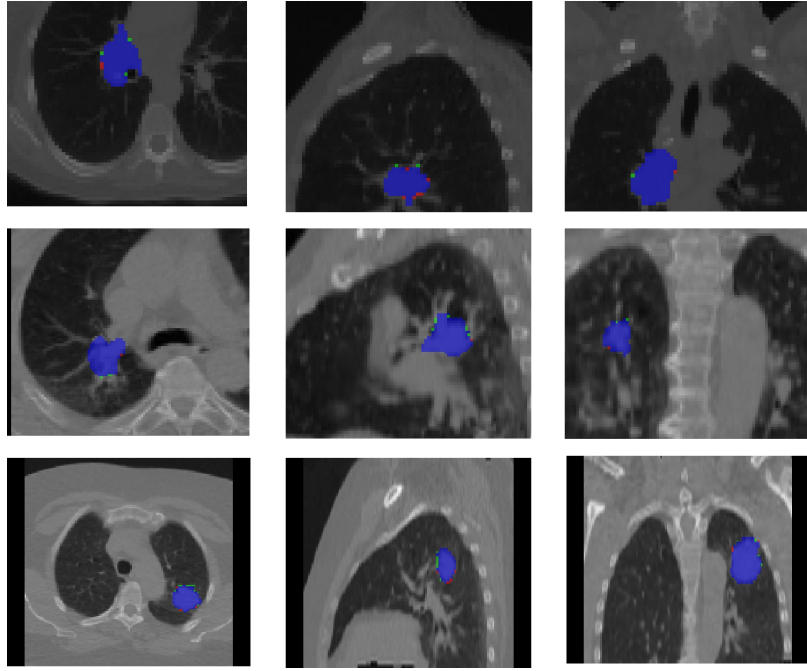


Fig 6 Visualization of tumor segmentation results. Red, blue and green indicate false negative, false positive and true positive, respectively.

3.2 Evaluation of robustness to noise

There is inevitable presence of artifacts (noise, scatter, etc.) in the real X-ray projection, which causes appearance disparity between the simulated DRRs and real X-ray projections. To investigate the effect of noise on the performance of the proposed method, according to previous work[4], we also evaluate the performance of RT-SRTS on noisy testing projection data by adding Gaussian noise with sigma ratio of 0.01, 0.02, and 0.05, while the model is trained on DRRs without adding noise.

Table 1 presents the performance metrics of the model under various noise levels.

Although there's a minor degradation in the reconstruction as the noise level increases, the results remain largely consistent. Similarly, the accuracy of segmentation

encounters a slight decline for noisy projections, but again, the outcome is comparable.

As shown in Fig 7, there is only minor difference between different reconstruction and segmentation results.

Table 1. Metric values of the 3D images generated by RT-SRTS from projection data added with Gaussian noise of varying sigma ratios.

Ratio	Reconstruction				Segmentation		
	MAE	MSE	RMSE	PSNR (dB)	SSIM	DICE	COMD (mm)
0	0.014	0.0005	0.074	35.47	0.966	0.960	0.31
0.01	0.016	0.0006	0.089	34.31	0.949	0.942	0.38
0.02	0.017	0.0006	0.097	33.45	0.949	0.944	0.39
0.05	0.019	0.0009	0.109	32.23	0.936	0.945	0.43

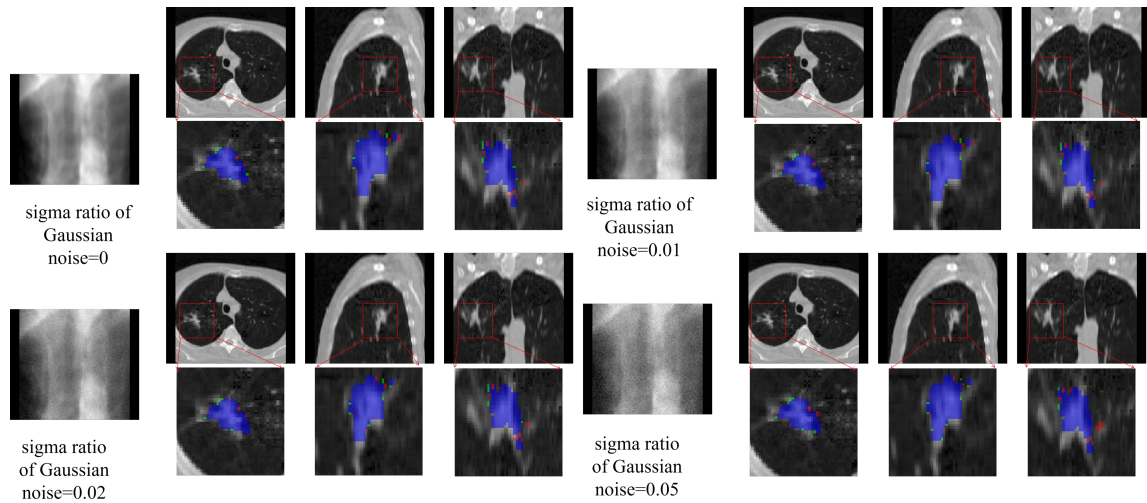


Fig 7 Visualization of noisy projection data and their corresponding reconstruction and segmentation results.

3.3 Ablation Study

Table 2. The results of the ablation study

		Reconstruction					Segmentation	
AEC	URE	MAE	MSE	RMSE	PSNR (dB)	SSIM	DICE	COMD (mm)
		0.017	0.0007	0.114	32.07	0.943	0.934	0.30
√		0.016	0.0005	0.081	34.89	0.960	0.943	0.31
√	√	0.014	0.0005	0.074	35.47	0.966	0.960	0.31

Ablation study is conducted to validate the effectiveness of the proposed AEC module and URE module. As shown in Table 2, it can be observed that there is a significant improvement in all metrics by adding the AEC and URE modules. Specifically, the AEC module provides significant improvement for reconstruction metrics such as PSNR, while the URE module contributes to a greater enhancement in segmentation DICE. By adopting the AEC module, the performance of reconstruction gains 2.81 dB in PSNR and 2% in SSIM. Equipped with the URE module in segmentation branch, the DICE is increased from 0.943 to 0.960.

4 Conclusion

In conclusion, this paper addresses the limitations of existing patient-specific CNN imaging methods in meeting the motion control requirements for VMAT radiotherapy. These methods fall short in terms of real-time tumor localization and are

only validated for fixed-angle imaging, which do not account for the rotating treatment beam and X-ray imaging system during beam delivery in VMAT.

To overcome these challenges, we propose a novel patient-specific CNN imaging RT-SRTS method that integrates 3D imaging and tumor segmentation into one network using the MLT strategy. This approach allows for simultaneous real-time 3D reconstruction and tumor segmentation. Besides, we introduce the attention enhanced calibrator (AEC) module, which effectively fuses hierarchical features with the imaging and segmentation branches, and leads to improved reconstruction and imaging results. Furthermore, the uncertain-region elaboration (URE) module is employed to enhance segmentation accuracy.

The effectiveness of RT-SRTS is evaluated in both fixed-angle and angle-agnostic imaging modes by comparing with two state-of-the-art methods. The results clearly demonstrate the superiority of RT-SRTS, achieving better results. Particularly noteworthy is the fact that RT-SRTS represents the first attempt to investigate direct 3D CT reconstruction from single X-ray projection at any angle using a single CNN imaging model.

Appendix A The testing results on ten cases

Table A1 The testing results of RT-SRTS on ten cases

	Tumor Size (cm ³)	Reconstruction				Segmentation		
		MAE	MSE	RMSE	PSNR (dB)	SSIM	DICE	COMD (mm)
Case1	6.96	0.0153	0.0004	0.0734	33.8817	0.9512	0.97392	0.456
Case2	0.119	0.0162	0.0006	0.0807	33.7997	0.9652	0.89075	0.155
Case3	0.313	0.0087	0.0002	0.0701	37.7828	0.9762	0.91732	0.163
Case4	2.470	0.0116	0.0003	0.0392	36.2180	0.9748	0.98867	0.155
Case5	3.020	0.0145	0.0004	0.1089	35.1537	0.9267	0.96940	0.052
Case6	5.252	0.0322	0.0016	0.1063	29.6960	0.9680	0.97569	0.122
Case7	1.434	0.0086	0.0002	0.0923	37.4820	0.9737	0.92827	0.239
Case8	12.70	0.0059	0.0001	0.0481	40.4013	0.9864	0.97337	0.220
Case9	3.563	0.0125	0.0003	0.0630	35.1389	0.9663	0.98666	0.467
Case10	26.90	0.0115	0.0003	0.0605	35.1817	0.9695	0.99229	0.422

Acknowledgments

This work was supported by the Beijing Natural Science Foundation (7232340 and L222034), the National Natural Science Foundation of China (61971443) and the Fundamental Research Funds for the Central Universities.

Declaration of Generative AI and AI-assisted technologies in the writing process

Statement: During the preparation of this work the authors used ChatGPT3.5 in order to improve readability and language. After using this tool, the authors reviewed and

edited the content as needed and takes full responsibility for the content of the publication.

CRedit authorship contribution statement

Miao Zhu: Conceptualization, Methodology, Writing - Original draft, Writing - review & editing, Data curation, Visualization, Validation. Qiming Fu: Investigation, Methodology, Writing - review & editing, Data curation, Visualization. Bo Liu: Investigation, Writing – review & editing, Data curation, Project administration, Supervision. Mengxi Zhang: Conceptualization, Methodology. Bojian Li: Data curation. Xiaoyan Luo: Writing – review & editing, Data curation. Fugen Zhou: Supervision.

Declaration of competing interest

Declaration of interest: The authors declares that there are no conflicts of interest.

Data availability

The primary patient data can be obtained at [SPARE Challenge – Image X Institute \(sydney.edu.au\)](https://www.sparechallenge.org/). Our code will be available at <https://github.com/ZywooSimple/RT-SRTS>.

References

1. Vinod, S.K. and E. Hau, *Radiotherapy treatment for lung cancer: Current status and future directions*. *Respirology*, 2020. **25**: p. 61-71.
2. Jafari, P., et al., *In-vivo lung biomechanical modeling for effective tumor motion tracking in external beam radiation therapy*. *Computers in Biology and Medicine*, 2021. **130**: p. 104231.
3. Keall, P.J., et al., *The management of respiratory motion in radiation oncology report of AAPM Task Group 76*. *Med Phys*, 2006. **33**(10): p. 3874-900.
4. Lei, Y., et al., *Deep learning-based real-time volumetric imaging for lung stereotactic body radiation therapy: a proof of concept study*. *Physics in Medicine & Biology*, 2020. **65**(23): p. 235003.
5. Wei, R., et al., *Convolutional neural network (CNN) based three dimensional tumor localization using single X-ray projection*. *IEEE Access*, 2019. **7**: p. 37026-37038.
6. Bertholet, J., et al., *Real-time intrafraction motion monitoring in external beam radiotherapy*. *Physics in medicine & biology*, 2019. **64**(15): p. 15TR01.
7. Meyer, P., et al., *Survey on deep learning for radiotherapy*. *Computers in Biology and Medicine*, 2018. **98**: p. 126-146.
8. Peng, T., et al., *Real-Time Markerless Tracking of Lung Tumors Based on 2-D Fluoroscopy Imaging Using Convolutional LSTM*. *IEEE transactions on radiation and plasma medical sciences*, 2021. **6**(2): p. 189-199.
9. Shieh, C.-C., et al., *Markerless tumor tracking using short kilovoltage imaging arcs for lung image-guided radiotherapy*. *Physics in medicine & biology*, 2015. **60**(24): p. 9437.
10. Hazelaar, C., et al., *Feasibility of markerless 3D position monitoring of the central airways using kilovoltage projection images: managing the risks of central lung stereotactic radiotherapy*. *Radiotherapy and Oncology*, 2018. **129**(2): p. 234-241.
11. de Bruin, K., et al., *Markerless real-time 3-dimensional kV tracking of lung tumors during free breathing stereotactic radiation therapy*. *Advances in Radiation Oncology*, 2021. **6**(4): p. 100705.
12. Shieh, C.-C., et al., *A Bayesian approach for three-dimensional markerless tumor tracking using kV imaging during lung radiotherapy*. *Physics in Medicine & Biology*, 2017. **62**(8): p. 3065.
13. Gendrin, C., et al., *Monitoring tumor motion by real time 2D/3D registration during radiotherapy*. *Radiotherapy and oncology*, 2012. **102**(2): p. 274-280.
14. Wang, M., et al., *2D/4D marker-free tumor tracking using 4D CBCT as the reference image*. *Physics in Medicine & Biology*, 2014. **59**(9): p. 2219.
15. Hugo, G.D., J. Liang, and D. Yan, *Marker-free lung tumor trajectory estimation from a cone beam CT sinogram*. *Physics in Medicine & Biology*, 2010. **55**(9): p. 2637.
16. Zhang, Q., et al., *A patient - specific respiratory model of anatomical motion for radiation treatment planning*. *Medical physics*, 2007. **34**(12): p. 4772-4781.
17. Li, R., et al., *3D tumor localization through real - time volumetric x - ray imaging for lung cancer radiotherapy*. *Medical physics*, 2011. **38**(5): p. 2783-2794.
18. Xu, Y., et al., *A method for volumetric imaging in radiotherapy using single x-ray projection*. *Medical physics*, 2015. **42**(5): p. 2498-2509.

19. Zhang, Y., et al., *A technique for estimating 4D -CBCT using prior knowledge and limited - angle projections*. Medical physics, 2013. **40**(12): p. 121701.
20. Shen, L., W. Zhao, and L. Xing, *Patient-specific reconstruction of volumetric computed tomography images from a single projection view via deep learning*. Nature Biomedical Engineering, 2019. **3**(11): p. 880-888.
21. Wei, R., et al., *Real-time tumor localization with single x-ray projection at arbitrary gantry angles using a convolutional neural network (CNN)*. Physics in Medicine & Biology, 2020. **65**(6): p. 065012.
22. Wei, R., et al., *A patient-independent CT intensity matching method using conditional generative adversarial networks (cGAN) for single x-ray projection-based tumor localization*. Physics in Medicine & Biology, 2020. **65**(14): p. 145009.
23. Wei, R., et al. *A CNN based volumetric imaging method with single X-ray projection*. in *2017 IEEE International Conference on Imaging Systems and Techniques (IST)*. 2017. IEEE.
24. Lu, S., et al., *Prior information-based high-resolution tomography image reconstruction from a single digitally reconstructed radiograph*. Physics in Medicine & Biology, 2022. **67**(8): p. 085004.
25. Ying, X., et al. *X2CT-GAN: reconstructing CT from biplanar X-rays with generative adversarial networks*. in *Proceedings of the IEEE/CVF conference on computer vision and pattern recognition*. 2019.
26. Ge, R., et al., *X-CTRSNet: 3D cervical vertebra CT reconstruction and segmentation directly from 2D X-ray images*. Knowledge-Based Systems, 2022. **236**: p. 107680.
27. Tan, Z., et al., *Semi-XctNet: Volumetric images reconstruction network from a single projection image via semi-supervised learning*. Computers in Biology and Medicine, 2023. **155**: p. 106663.
28. Evangelista, D., E. Morotti, and E.L. Piccolomini, *RISING: A new framework for model-based few-view CT image reconstruction with deep learning*. Computerized Medical Imaging and Graphics, 2023. **103**: p. 102156.
29. Tan, Z., et al., *XctNet: Reconstruction network of volumetric images from a single X-ray image*. Computerized Medical Imaging and Graphics, 2022. **98**: p. 102067.
30. He, K., et al. *Deep residual learning for image recognition*. in *Proceedings of the IEEE conference on computer vision and pattern recognition*. 2016.
31. Vaswani, A., et al., *Attention is all you need*. Advances in neural information processing systems, 2017. **30**.
32. Zhang, Y., et al. *Multi-phase liver tumor segmentation with spatial aggregation and uncertain region inpainting*. in *Medical Image Computing and Computer Assisted Intervention—MICCAI 2021: 24th International Conference, Strasbourg, France, September 27–October 1, 2021, Proceedings, Part I 24*. 2021. Springer.
33. Shieh, C.C., et al., *SPARE: Sparse -view reconstruction challenge for 4D cone -beam CT from a 1 -min scan*. Medical physics, 2019. **46**(9): p. 3799-3811.
34. Keiper, T.D., et al., *Feasibility of real-time motion tracking using cine MRI during MR-guided radiation therapy for abdominal targets*. Medical Physics, 2020. **47**(8): p. 3554-3566.